Particle Re-Deposition During Ultrashort Pulse Laser Ablation of ITO Thin Films Using Single- and Multi-Beam Processing

Jana Köller*[1,2], Astrid Sassmannshausen[2], Martin Kratz[1,2], and Jan Voß[1,2]

[1]*Fraunhofer ILT - Institute for Laser Technology, Steinbachstr. 15, 52074 Aachen, Germany*
[2]*RWTH Aachen University LLT - Chair for Laser Technology, Steinbachstr. 15, 52074 Aachen, Germany*
[*]*Corresponding author's e-mail: jana.koeller@ilt.fraunhofer.de*

The processing of transparent conductive oxides (TCO) using ultrashort laser pulses (USP) is of interest for an increasing number of applications. Among other things, the coupling of the energy into the workpiece is crucial for the precise machining of materials. To this intent, the effects of pulse duration, fluence, numerical aperture (NA), pulse overlap, beam shaping, and a suction system on particle re-deposition are investigated during partial ablation of a 100 nm thick indium tin oxide (ITO) layer on fused silica. It is shown that in particular, a large NA and therefore a small spot diameter as well as a high pulse overlap significantly influence the re-deposition of particles regarding their amount, size and local distribution on the sample surface. Furthermore, the beam shaping and the resulting multi spots show an effect on the particle dynamics during a machining process.
DOI: 10.2961/jlmn.2022.03.2007
Keywords: materials processing, transparent conductive oxides, particle re-deposition, ultrashort pulse, energy coupling, shielding

1. Introduction

Indium tin oxide (ITO) is one material from the group of transparent conductive oxides (TCO). These materials are particularly characterized by their high conductivity and transparency in the visible spectrum. Their range of application extends from the production of conductive electrodes and solar cells to building insulation and touch panels [1–4]. It has already been shown that high precision and surface quality are required when processing conductive layers of ITO for generating interconnect lines, for example, to ensure the performance of devices such as OLEDs [5,6]. Conventionally, patterning of ITO electrodes has been performed by photolithography processes, but several process steps are required [7]. Ultrashort pulse laser processing is therefore especially advantageous due to its very high accuracy, low heat impact and high flexibility [8]. To provide and control laser material processing of thin ITO films using ultrashort laser pulses, a large number of researchers have already investigated fundamental mechanisms. These include the influence of fluence, pulse duration and pulse overlap on the ablation result. On the one hand, it is found that a higher pulse duration also reduces the linewidth and, on the other hand, that the scan speed and thus the pulse overlap is decisive for the complete removal of the coating without damaging the glass substrate beneath the ITO layer [9]. It has also been shown by Farid et al. that a higher pulse overlap decreases the resulting edge width and increases the linewidth [10]. The decreasing linewidth with increasing scan speed, respectively with decreasing pulse overlap could also be found by other research groups [11–13]. However, it is already known that processing with laser radiation can also lead to problems concerning crack formation or the deposition of ablation particles and material residues to form short circuits. The deposition of particles can also contaminate the surrounding material. These effects were found by Harrison et al. when processing with a laser in the ns range. [14] The ridge minimization at the crater rims depending on the beam shape used has already been investigated. The use of a quasi-flat top beam showed a lower throw-up than a laser spot with a Gaussian profile. The avoidance of ridges is important to prevent short circuits. [15] Park et al. were able to show, in comparison to previous literature, that these ridges are significantly reduced by the use of ultra-short laser pulses alone. [16]. For a more detailed analysis of the ablation behavior of thin ITO films on glass, Hallum et al. looked at the ablation process using reflective pump-probe microscopy. It is assumed that the first step is the bulging and ablation by spallation of a part of the layer. With increasing pulse peak fluence a transition to phase explosion is observed. [17]

Particle re-deposition is studied for different laser parameters, including pulse duration, fluences, and numerical aperture (NA). The NA and the pulse duration play a decisive role with regard to the thermal damage of the surrounding material. Small laser spots result in significantly less thermal influence on the surrounding material due to their steep flank, which means that less energy that cannot contribute to the ablation process remains in the material in the form of heat. However, these small spot diameters lead to low productivity, although this can be increased by using multi-beam patterns. Therefore, the change and influence of the particle re-deposition and dynamics by using different multi-beam patterns is also analyzed. The deposition and dynamics of particles, as well as their control and avoidance during the ablation process, are not understood yet. However, particles reduce component quality and can even render components unusable, for example through short circuits.

Therefore, the understanding as well as the avoidance of particle redeposition in critical regimes and control of particle dynamics is crucial for high quality fabrication of components. In the following chapter 2 the theoretical background of different ablation mechanisms in the processing of materials with ultrashort pulsed (USP) laser radiation is explained, as well as subsequently in chapter 3 the methods used. This includes both the experimental setup and the materials, as well as the measurement methods. In the main part, chapter 4, the obtained results of particle re-deposition by utilizing single and multi-beam intensity distributions are presented.

2. Theoretical background

In the ablation of material using pulsed laser radiation, a distinction is made between thermal and non-thermal or photomechanical ablation mechanisms.

For ultrashort laser pulses (**Fig. 1**) the incident pulse is over until the introduced energy has heated and ablated the material. The first step of energy transfer takes place from the photons of the laser pulse to the electrons. But the transfer from the electrons to the phonons occurs on a longer time scale than the pulse duration, resulting in the use of the two-temperature model [18]. Due to the short pulse duration, significantly lower temperatures are reached in the material. Shielding or accumulative effects can occur for ultrashort pulse durations with the subsequent pulse.

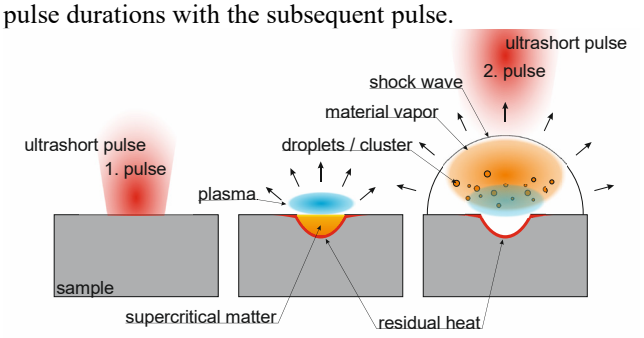

Fig. 1 Thermal ablation with ultrashort laser pulses

For ultrashort laser pulses, mechanical ablation of the material dominates, since energy is deposited in the material in a very short time, resulting in high temperature gradients. Due to these high temperature gradients, a strong stress is generated in the material, which leads to ablation of the material. Here, the ablation process with ultrashort laser radiation is shown as an example for a bulk material. For the ablation of thin layers, the dominance of mechanical ablation as well as the shielding or accumulation of the laser pulses is also relevant. In the following figure **Fig. 2**, the mechanical ablation for a thin film layer system is shown in a schematic sketch. After the shock waves and stress have detached the thin film from the substrate, the material bulges and then breaks up into small particles which stay above the processed area. Similar observations as Rapp et. al. [19] were made by Hallum et al. who investigated the ablation process by reflective pump-probe microscopy for thin ITO layers on glass. Here, too, it can be assumed that the layer or part of the layer bulges and then fragments. [17]

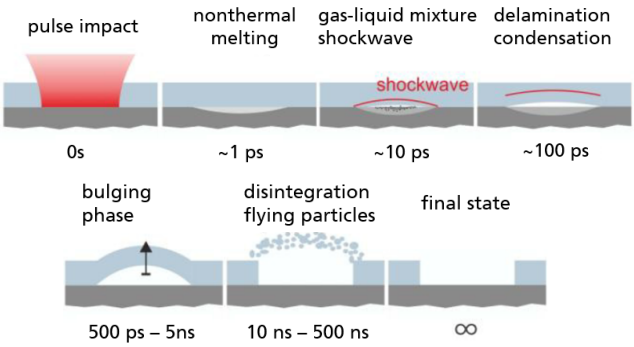

Fig. 2 Mechanical ablation with ultrashort laser [19]

These particles generated by the ablation process are studied in this paper in terms of their dynamics and how they are affected by the laser parameters.

3. Methods

In this chapter the materials, setups and measurement methods used, as well as some information about the processes are explained.

3.1 Experimental Setup and materials

The laser beam (laser source: TruMicro2000 system, TRUMPF) is directed through a half-wave-plate and mirror onto the spatial light modulator (SLM). A 4F system is used and the laser beam is imaged into the micro scanner. All the components needed to use an SLM are attached to the plate drawn in gray here. Since the distance between the SLM and the microscope objective is fixed, the entire gray plate is moved in this setup.

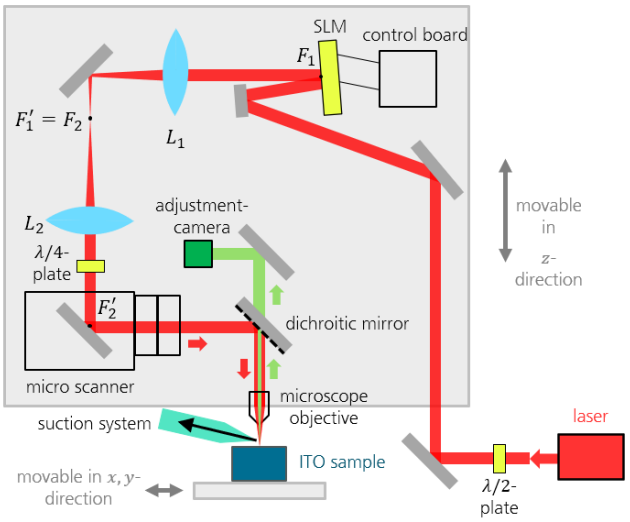

Fig. 3 Experimental setup

The laser beam is focused on the sample surface via a dichroitic mirror and a microscope objective or lens. A suction system (ULT – LAS 260 HD.19FK at 60% max. flow) is used for the targeted suction of the particles in the process, whereby the sample is positioned and moved on a xy axis system. All tests are carried out once with and once without extraction of the particles in order to investigate the effect of active suction. The SLM (liquid crystal on silicon-spatial light modulator (LCOS-SLM) X11840-09(X), Hamamatsu) is used for the generation of multi-beam intensity distributions and the flexible arrangement of the laser beams. is the

different intensity distributions are generated by using phase masks. These phase masks are generated according to the principle of Gerchberg and Saxton's iterative Fourier transform algorithm (IFTA) [20] and camera feedback. The parameters of the laser are listed in **Table 1**, including both constant parameters and varied values. Two pulse durations and NAs, four pulse overlaps as well as different fluences between 0.5 J/cm² and 4 J/cm² are used.

Table 1 Laser parameter

Parameter	Value
Wavelength λ	1030 nm
Pulse duration τ	0.4 or 10 ps
Pulse repetition rate f_{rep}	25 kHz
Average power P	Max. 20 W
Max. peek pulse fluence F	0.5 to 4 J/cm²
Intensity I	5.3 to 43 × 10^{11} W/cm²
Spot diameter $2w_0$	4 or 25 µm
Numerical aperture NA	0.04 or 0.29
Pulse overlap	70%, 80%, 90%, 99%

In this paper, fluence is always used for the case of the peak pulse fluence of a single pulse. The used pulse overlap and peak pulse fluence result in the accumulated fluence.

The ITO is a thin layer of approximately 100 nm on a quartz glass substrate. The film thickness is determined by measuring it in the cross section of the sample using a scanning electron microscope (SEM), and the uniformity of the coating was verified to exclude strong variations of the film thickness on the substrate.

3.2 Process principle and scanning strategy

The fluence distribution of the laser beams follows a gaussian distribution. The specified fluence always refers to the maximum peak pulse fluence.

The fixed laser spot diameter, determined at the point where the intensity drops to 1/e², and the speed of the axis create a fixed pulse overlap (PO) that can be changed by varying the speed. This becomes larger with decreasing speed and leads to the ablation of a line with large pulse overlaps, depending on the spot diameter. In addition to the scan speed and the spot diameter, the repetition rate is a key parameter for the pulse overlap. If the other two parameters are left constant and only the repetition rate is increased, this results in a higher pulse overlap, so that a higher scan speed must be used to achieve the same value.

$$PO = \left(1 - \frac{v_s}{2w_0 \cdot f_{rep}}\right) \cdot 100\% \qquad (1)$$

3.3 Measuring methods

A non-contact atomic force microscopy in amplitude modulation mode (AFM) from the company BRUKER is used to determine the generated cavities.

The second method is a SEM to generate high-resolution images of the particles (**Fig. 5**). Subsequently, these images are evaluated by an automated analysis with respect to the size and position of the particles.

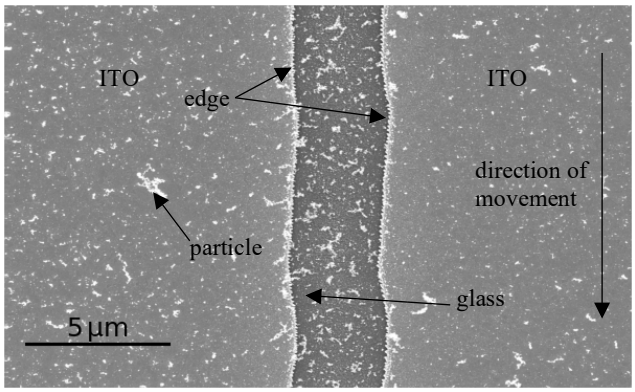

Fig. 4 Example SEM image of particles

When measuring the absolute depth of the cavities with the WIM, sometimes depths smaller than 100 nm or even larger are indicated. However, for these ablation geometries, no damage to the glass is visible in the SEM images. Furthermore, a planar plateau region, as shown in **Fig. 4** on the right, is mainly expected when there is a transition to an underlying material with a higher ablation threshold, but which has not yet been ablated.

4. Results and discussion

In the discussion of the results in this chapter, a distinction is made between the analysis of the influences of the laser parameters on particle deposition in single-beam and multi-beam ablation.

4.1 Single beam ablation

In this chapter the experiments with a single beam and the variation of the parameters pulse overlap, pulse duration, numerical aperture, fluences are investigated with respect to the influence on the particle deposition. In addition, the effect of suction on particle deposition is also analyzed. Unless otherwise indicated, all images and results have been performed without suction.

Pulse overlap

The first parameter analyzed is the pulse overlap, with all other parameters held constant (see **Fig. 6**).

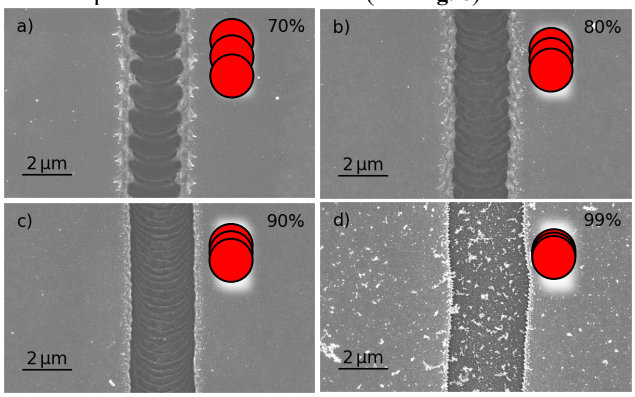

Fig. 5 SEM figure with τ =0.4 ps, $2w_0$=4 µm, F=1.4 J/cm² and a) 70%, b) 80%, c) 90% and d) 99% pulse overlap. The red dots schematically represent the change in pulse overlap.

This shows that with a percentage overlap of 70% with the following pulse, the influence of each individual pulse is distinguishable. In addition, ejections and deposits of the

material directly at the edge of the cavity are visible. With increasing pulse overlap, smaller and fewer material ejections are observed at the crater rims. However, the influence of the individual pulses shows up to 90% pulse overlap and disappears only at 99%, whereas here a strong re-deposition of particles in the µm range with a flake-like shape can be observed. These particles at 99% suggest a change in the ablation mechanism due to the increased overlap of the pulses.

In the case of ablation with a single-beam, the particles here act symmetrically distributed over the pristine and processed surface. In the direct cross-section comparison of the height profile between a pulse overlap of 80% and 99% the crater geometry differs noticeably (see **Fig. 7**). Here, both a greater depth and a parabolic course are achieved with 80%, whereas ablation with 99% leads to a nearly flat plateau area in the center of the cavity with a small throw-up in the center, which may also be due to the deposited particles.

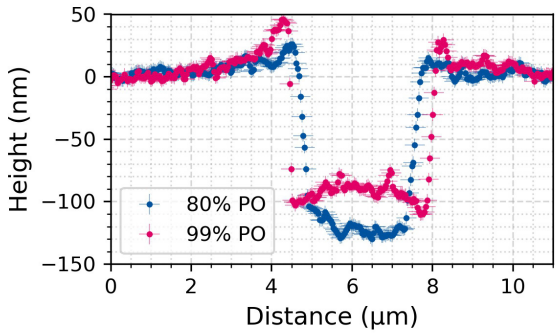

Fig. 6 AFM height profile with τ =0.4 ps, $2w_0$=4 µm, F=1.4 J/cm² and 80% (blue) and 99% (red) pulse overlap

In this context, it is reasonable to assume that due to the generated particles not all the energy of the laser pulses hits the material. Thus, by providing a small overlap when a homogeneous ablation region is not required, the generation of larger flake-like particles can be avoided. Unevenness due to detached material remains here at the crater edge. Since the depth for 80% is about 123 +/- 5 nm, it can be assumed that the glass is damaged, even if there is no clear indication of glass damage in the corresponding SEM images. The selected parameters of 1.4 J/cm² and a repetition rate of 25 kHz normally exclude damage to the glass, since the threshold fluences for fused silica is above 3 J/cm² [21] for single pulses and heat accumulation, which favors melting of the material, only occurs above around 100 kHz. The fact that less material is removed when using 99% pulse overlap than with 80% can be explained by the shielding effect of the particles that occur. As a result, the entire energy of each pulse no longer reaches the material surface.

Pulse duration

As a second parameter, the influence of the pulse duration on the generated particles is investigated. A short pulse duration of 0.4 ps and a longer one of 10 ps are utilized (see **Fig. 8**). Significantly less particles are observed when τ = 10 ps, and the type is also different from the previous particles that were addressed when varying the pulse overlap at short pulse duration of τ = 0.4 ps. Here, the particles are significantly smaller and more likely to be in the nm range, and they also have a granular shape.

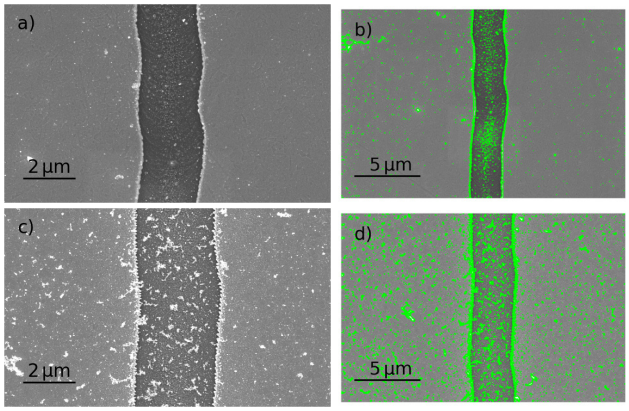

Fig. 7 SEM figure with $2w_0$=4 µm, F=1.4 J/cm², 99% pulse overlap and a), b) τ =10 ps and c), d) τ =0.4 ps with associated detections of the contours in the hole image (right, b) and d))

This different particle generation during the ablation process also suggests that different ablation mechanisms dominate and probably also lead to these two different types of particles. Whereas at a pulse duration of τ = 10 ps, it is reasonable to assume that thermal mechanisms have a greater influence than at τ = 0.4 ps.

However, when the fluence is increased, nearly identical results are obtained for τ = 10 ps and τ = 0.4 ps in terms of particle deposition and arrangement (see **Fig. 9**). This suggests that fluence also has a decisive influence on the ablation mechanisms and that this influence overrides the influence of pulse duration with increasing fluence.

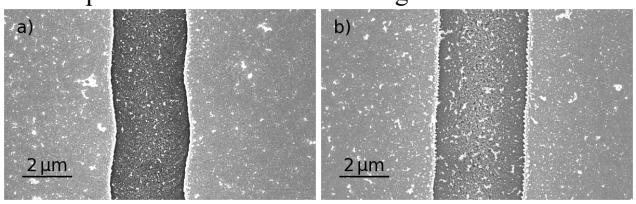

Fig. 8 SEM figure with $2w_0$=4 µm, F= 2.5 J/cm², 99% pulse overlap and a) τ =10 ps and b) τ =0.4 ps

Numerical aperture

When using a small NA, this results in a larger spot diameter in this case of $2w_0$ = 25µm and a weaker focusing. This weaker focusing results in a greater thermal influence in the area of the edges of the pulse (see **Fig. 10**).

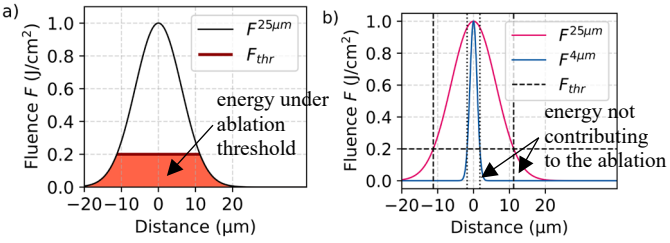

Fig. 9 Schematic sketch of fluence distribution and threshold fluence a) with marked area where the energy is under the ablation threshold and b) for different focusing by small and large NA with marked edge areas under the threshold

A larger fraction of the pulse energy lies between the intersection of the threshold fluence with the fluence profile of the pulse (vertical dashed lines for both spot diameters in **Fig. 10**b) and the edge of the pulse. The arrows in **Fig. 10**b indicate these areas, where the energy fraction between the

vertically dashed lines and the flank is larger for large spot diameters. What exactly happens to this portion of the energy in the process depends on the dominant absorption mechanisms. In the case of non-linear mechanisms, the energy would pass through the material below the threshold, whereas in the case of linear absorption mechanisms, it would remain in the material as heat. In addition, the wider flanks cause wider edges at the cavity.

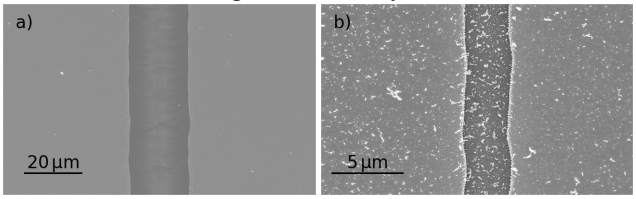

Fig. 10 SEM figure with F=1.4 J/cm², 99% pulse overlap, τ =0.4 ps and spot size a) $2w_0$=25 µm (NA 0.04) and b) $2w_0$=4 µm (NA 0.29)

When evaluating the SEM images (see **Fig. 11**), it is noticeable that no particles in the µm range are produced when a large spot diameter is used, as is the case when a small spot diameter is used. This difference is probably due to the different ablation mechanisms, as it is already the case with the pulse duration. With a strong and therefore very local energy input, such as with a $2w_0$ = 4 µm, higher stresses are produced in the material, which lead to increased mechanical ablation of the material. On closer inspection, it is noticeable that tiny granular particles in the nm range have been created in the cavity.

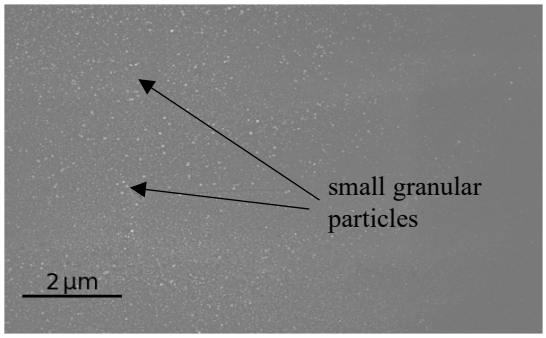

Fig. 11 Detail view of the cavity of **Fig. 11** a) with F=1.4 J/cm², 99% pulse overlap, τ =0.4 ps and $2w_0$=25 µm (NA 0.04)

Long pulse durations and large spot diameters thus appear to produce some of these granular-small particles, suggesting that thermal effects play a somewhat larger role here and favor the generation of this type of particle.

Fluence

By varying the pulse peak fluence, it can be observed that, on the one hand, the ablated lines widen, since a wider pulse range lies above the threshold fluence and thus contributes to ablation (see **Fig. 13**). It is also visible that as the fluences increase, the brightness around the cavity increases. This may indicate that small, granular particles are also increasingly deposited here, which are observed before with a large NA and a long pulse duration. At low fluences of 0.5 J/cm², larger particles still adhere directly to the edge of the ablated cavity. In contrast, as the fluence increases, the particles look smaller and their number increases. Thus, both types of particles are found even at short pulse durations

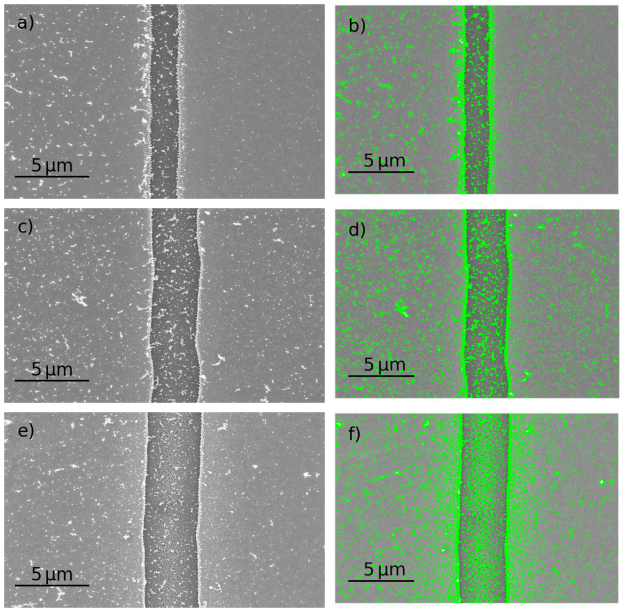

Fig. 12 SEM figure with 99% pulse overlap, τ =0.4 ps, $2w_0$=4 µm (NA 0.29) and a) F=0.5 J/cm², c) F=1.4 J/cm² and e) F=2.5 J/cm² with associated detections of the contours (right)

This result can be illustrated by evaluating the detected contours and thus the calculated size of the particles, their position and their number. Here, the histograms in **Fig. 14** each belong to the images previously shown in the rows in **Fig. 13**. The data in histograms **Fig. 14**a) and b) belong to **Fig. 13**a) and b), where in **Fig. 13** a) und b) the same images are shown and in b) additionally all detected particles are marked. The red vertical lines in the histograms on the left side of **Fig. 14** mark the edges of the cavity.

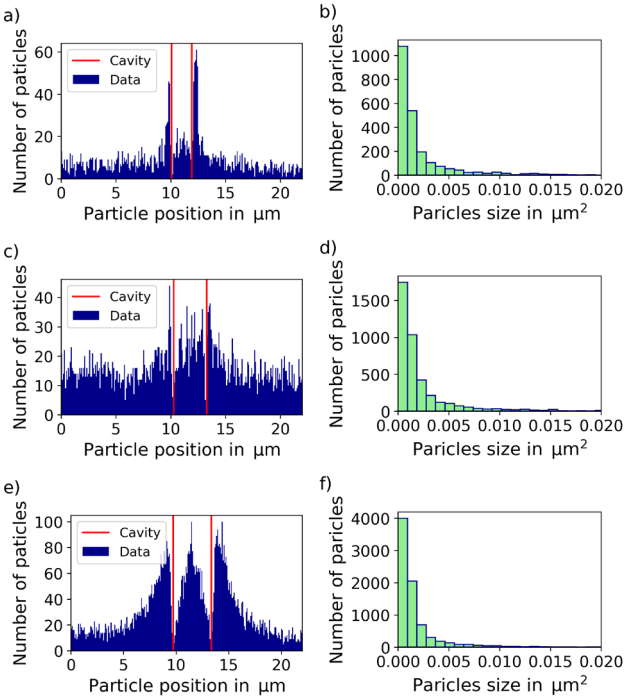

Fig. 13 Histogram of particle number over position (left) and size (right) for 99% pulse overlap, τ =0.4 ps and $2w_0$=4 µm (NA 0.29) a) and b) F=0.5 J/cm², c) and d) F=1.4 J/cm² and e) and f) F=2.5 J/cm²

The ablated area is located between the red lines. Even though on the images with the detection of the contours on the left in **Fig. 13** the crater edges are always completely marked as contours, these pixels have been excluded for the histograms, since here in most cases only the transition from ablated to not ablated led to detection. The particles adhere more strongly to the edge of the cavity at low fluences of 0.5 J/cm², which is also visible in **Fig. 14** a). With increasing fluence, **Fig. 14** c) shows an almost uniform distribution of the particles over the sample surface, and with high fluence of 2.5 J/cm² in **Fig. 14** e) an increased re-deposition in the center of the cavity as well as at the outer area of the edges of the cavity, which decreases with distance from the cavity, is seen. The fact that the particle number increases with increasing fluence, as can be seen in **Fig. 14** on the right, can have different reasons. On the one hand, more energy is coupled into the material at the same time, resulting in higher temperature gradients and stronger stress in the thin layer, whereby the layer no longer breaks into a few large pieces, but many small pieces. Thus, a slight change in the ablation mechanism may take place. On the other hand, higher fluences push the limits of the threshold fluences further to the edge of the pulse, so that the diameter that contributes to the removal of the material is larger than for small fluences. As a result, the areas in which the pulse encounters unprocessed material are smaller, which can promote smaller particle formation.

Suction system

After investigating the influence of different laser parameters on the generation and re-deposition of particles, a suction system will now be used during the experiments to find out whether this can remove the particles.

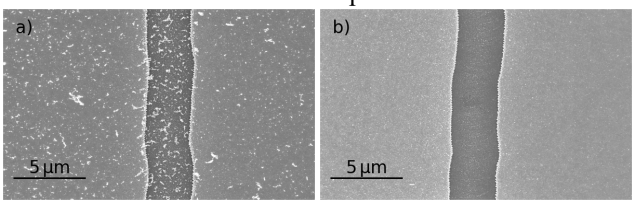

Fig. 14 SEM figure with F=1.4 J/cm², 99% pulse overlap, τ =0.4 ps and $2w_0$=4 µm (NA 0.29) and a) without suction and b) with suction

Flake-like particles in the µm range are observed (see **Fig. 15**), which can be seen in the left image, and can be sucked off. Only small granular particles, as in the right image, remain on the sample. It should be taken into account that the differences in brightness result from the images and therefore the small particles on the right appear much brighter in the image, but presumably, these are also found among the large flake-like particles in the left image. These are just not well visible because the larger particles overlay them and produce a stronger signal. In **Fig. 16** the small particles remaining on the sample are shown with a higher resolution. When ablating with only a single laser beam, the particles are expected to deposit symmetrically on the sample if no external conditions affect these dynamics. In some images, there seems to be a minimal tendency of the large particles to deposit on the left side, which may be caused by the environment and the flow box above the setup.

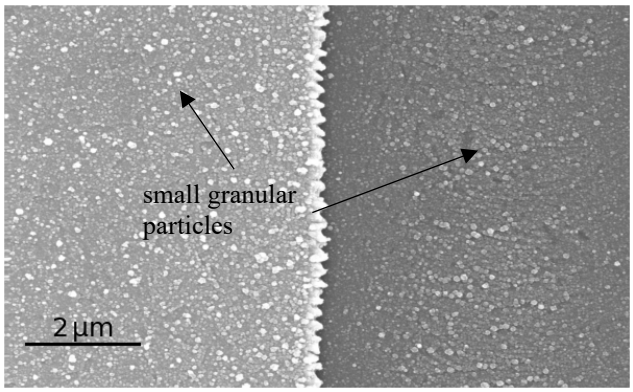

Fig. 15 SEM figure detailed view of **Fig. 15** b) with F=1.4 J/cm², 99% pulse overlap, τ =0.4 ps and $2w_0$=4 µm (NA 0.29) and with suction

4.2 Multi beam ablation

It has already been found that when a single beam is used, the flake-like particles in the µm range are produced mainly due to short pulse durations, small spot diameters and the absence of suction. In addition to the large particles, small particles in the nm range were also found. These also occur with longer pulse durations and a large spot diameter. Due to the advantages of small spot diameters and short pulse durations already mentioned above, these are used for multi-beam distribution, as is the pulse overlap of 99%, which enables uniform ablation.

To increase productivity in materials processing with small laser spots, ablation can be performed with multi-beams which simultaneously process the material. The arrangement of these beams depends on the required conditions, for example whether a single wider line with several small spots or several small lines next to each other are to be ablated. The interaction between simultaneous ablation centers increases the complexity of particle generation and re-deposition. Based on the previous results for single-beams the influence of two different symmetries of laser spots on the dynamics of particle re-deposition is investigated here.

V-shape without suction

7 laser spots are arranged in a V-shape, as shown in **Fig. 17**. The aperture angle α can be adjusted and is varied between 6° and 30°.

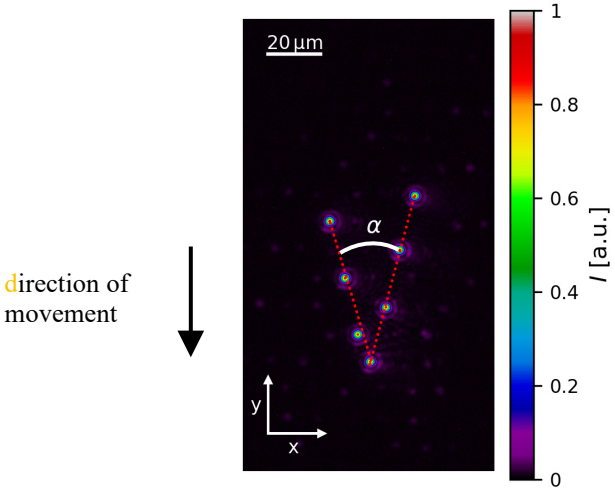

Fig. 16 Arrangement of 7 laser spots in the V-shape

Ablation with this spot arrangement clearly shows that small particles in particular, which can be seen in **Fig. 18** due to a higher brightness in the areas of increased deposition, are deposited in the center of the cavity. The larger particles in the µm range are distributed over the entire sample surface, whereby it is noticeable that fewer small or large particles are found in the track on the far right than in the track on the far left.

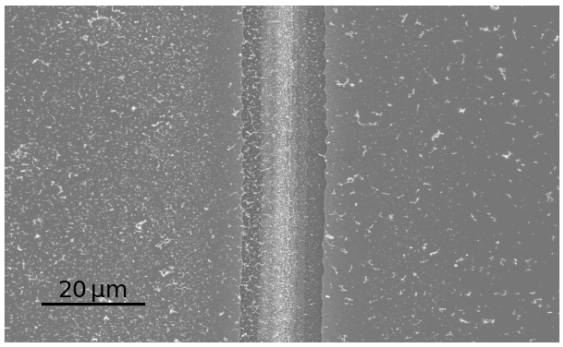

Fig. 17 SEM image of the ablation result with F=1.4 J/cm², 99% pulse overlap, τ =0.4 ps and $2w_0$=4 µm, 12° angle and V-shape

In addition, the particles on the far left and right next to the cavity look more flake-like, whereas towards the center they become smaller and show the strongest re-deposition in the center. A detailed image of the cavity with its particles from **Fig. 18** is shown in **Fig. 19**.

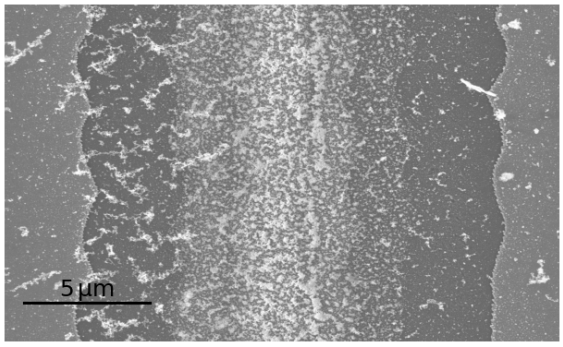

Fig. 18 SEM image detailed view of **Fig. 16** of the ablation result with F=1.4 J/cm², 99% pulse overlap, τ =0.4 ps and $2w_0$=4 µm, 12° angle and V-shape

The approximate symmetrical distribution of the particles can be explained by the nearly symmetrical arrangement of the spots. The influence of these seven laser spots on the particle dynamics is shown schematically in the sketch in **Fig. 20**. The laser spot in the center of the V is the first one which hits the unprocessed material and generates particles.

In this case, these particles are drawn as a cloud above the material. Whether and how long these particles remain in the air or are deposited on the surface of the material when the following spot reaches this point cannot be clearly stated at this point. For this, subsequent in-situ recordings are helpful to understand the time-resolved dynamics.

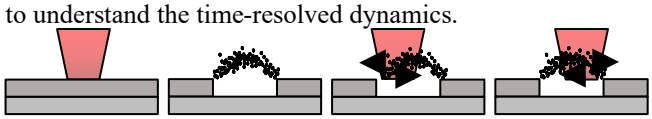

Fig. 19 Systematic sketch for influencing the particle re-deposition when arranging the spots in a V-shape

In this arrangement, the pulses following the first laser spot push the particles into the center of the cavity. The laser spots following the first one, shifted slightly to the left and then slightly to the right, ensure that a larger proportion of the particles are pushed to the center. This area is being limited by the bordering spots on the opposite side. These particles in the center are hit more frequently by laser pulses than particles that are pushed directly outward and thus lie outside the geometry, including all seven laser spots. This results in an increased deposition of smaller particles in the center of the cavity. The reduction in particle size can be explained by the increased impingement of other pulses on the particles. The areas of the sample outside the geometry show a uniform particle distribution. The re-deposited particles decrease from the center of the cavity to the outside within the tracks. The reason for this is the arrangement of the spots, whereby the spots are further away from the center, the later they contribute to the dynamics and are also further out, which means that the particles have more surface area to distribute themselves. The fewest particles in the right track produced by the outer right laser spot can be explained by the fact that this spot is the last one to process the material in terms of time and thus causes a final decisive push in the dynamics. The propagation of the generated particles is not limited in any direction or the particles are hit a second time by a following laser spot.

V-shape with suction

If suction is used in the ablation process, most of the larger particles in the µm range can be removed, as with ablation with a single laser spot, but small particles remain on the sample (see **Fig. 21**).

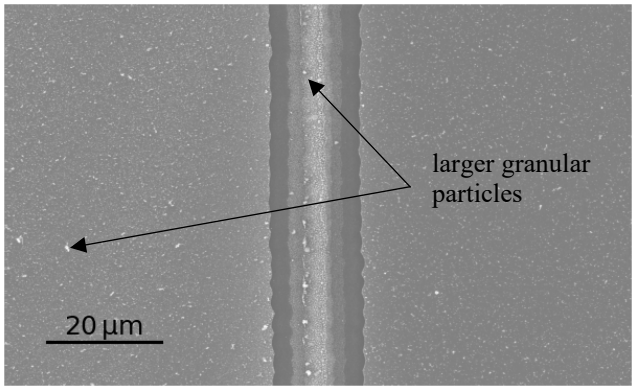

Fig. 20 SEM image of the ablation result with F=1.4 J/cm², 99% pulse overlap, τ =0.4 ps and $2w_0$=4 µm, 12° angle, suction and the arrangement in a V-shape

The remaining particles are symmetrically distributed and sometimes appear larger than the granular, round particles found during processing with a single laser spot. It can be assumed that some of the particles adhere more strongly to the surface or that smaller flake-like particles have been compressed and therefore no longer have the same surface area at the same weight, which means that the extraction system can no longer remove them.

If a larger opening angle is selected, separate lines are generated instead of a continuous cavity, as shown in **Fig. 22**. In this case, there is a weaker deposition of particles. But here, too, not only the granular particles are visible, as in the case of ablation with a single laser spot, but also a homogeneous

and symmetrical deposition of somewhat larger particles, which were also previously detected at 12° aperture angle.

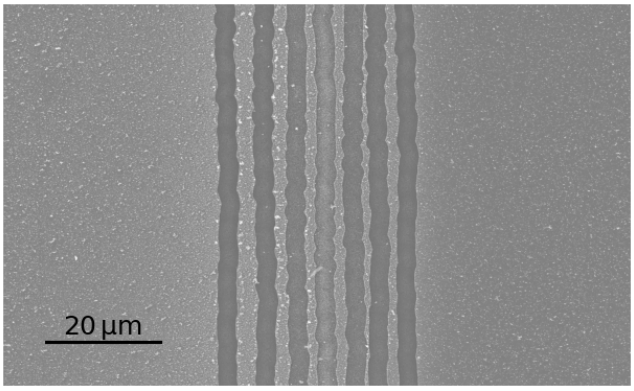

Fig. 21 SEM image of the ablation result with F=1.4 J/cm², 99% pulse overlap, τ =0.4 ps and $2w_0$=4 µm, 30° angle, suction and the arrangement in a V-shape

It becomes clear that even at larger aperture angles, which lead to one line per laser spot, the particle dynamics are influenced by the different spots and lead to a slightly different deposition than with a single spot. However, the interaction is weaker than with a small angle.

Flank shape without suction

By using an asymmetric spot arrangement in the form of a flank, the dynamics of the particle re-deposition can be controlled in a more targeted manner, whereby here the center of gravity of the deposits is no longer to be expected in the center of the cavity, but rather on the left side.

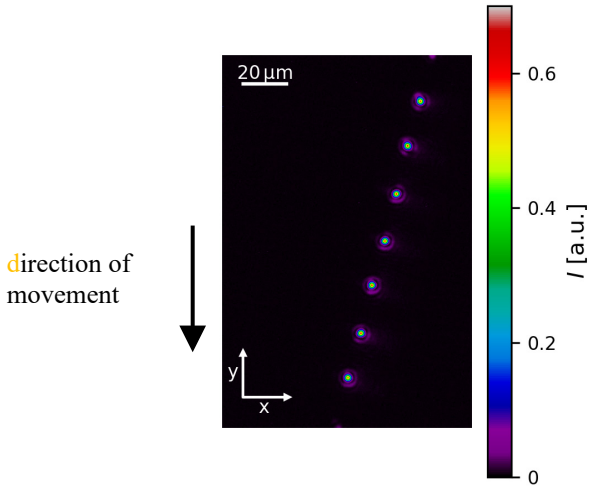

Fig. 22 Arrangement of 7 laser spots in the shape of a flank

Only one side of the V is used for this purpose, but now 7 laser spots are arranged on one side, as can be seen in **Fig. 24**. The particles are pushed more to the left side, as expected (see **Fig. 24**). In addition, it is particularly noticeable that the particles on the left side are smaller and present in greater numbers than on the right side of the cavity.

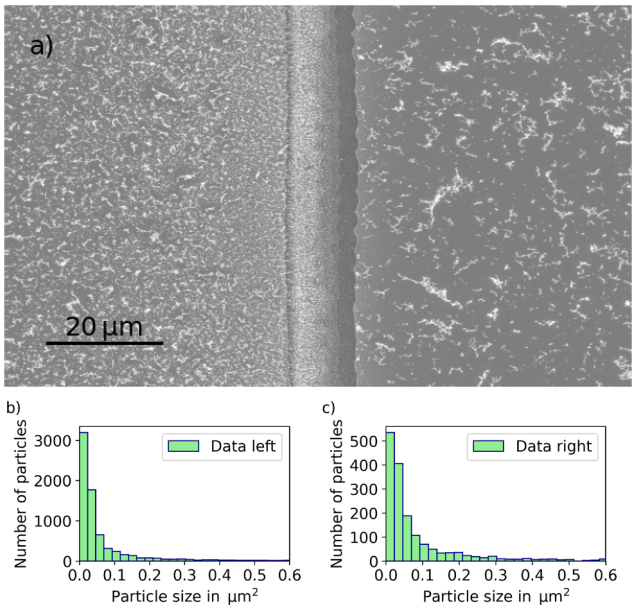

Fig. 23 SEM image of the ablation result with F=1.4 J/cm², 99% pulse overlap, τ =0.4 ps and $2w_0$=4 µm, 12° angle, without suction and the arrangement in a flank-shape. The histograms show the number of particles against the size on the b) left and c) right side of the cavity

The distribution of the particles to the left side is caused by the fact that after the first spot all following spots on the right side follow and thus a limitation of the dispersion of the particles is present so that these disperse further in the left direction and deposit (see **Fig. 25**). The differences in particle size depending on the side of the cavity considered may be because the laser pulses on the right side always hit material that is still unmodified, whereas on the left side particles have already been generated by previous laser spots and the material has been removed. By repeatedly hitting the particles with laser pulses, the size can be reduced and the number increases.

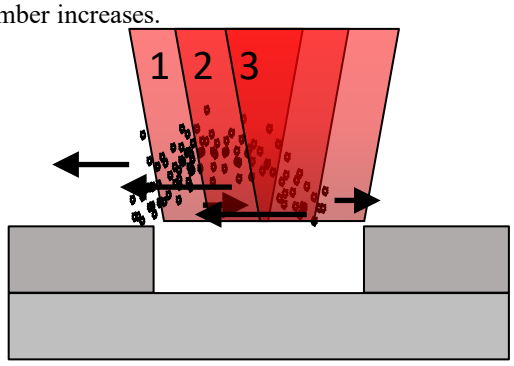

Fig. 24 Systematic sketch for influencing the particle re-deposition when arranging the spots in a flank-shape

Flank shape with suction

If suction is now also used during the process, all larger flake-like particles can be extracted, as previously noted. An increased re-deposition of particles remains, especially on the left side of the cavity. However, as with the V-shape, it is observed that some larger particles remain on the surface. The right side of the cavity is almost free of particles (see **Fig. 26**).

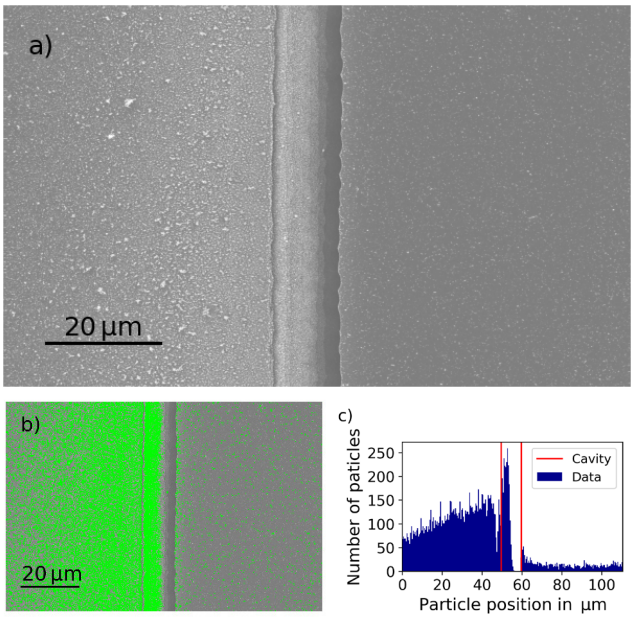

Fig. 25 a) SEM image of the ablation result with F=1.4 J/cm², 99% pulse overlap, τ =0.4 ps and $2w_0$=4 µm, 12° angle, with suction and the arrangement in a flank-shape, b) with associated detections of the contours and c) histogram of particle number over position

5. Conclusion and outlook

In conclusion, two different types of particles are produced by the ablation processes and are deposited on the machined and unmachined surfaces. On the one hand, flake-like particles are produced in the µm range, which can be removed by suction. On the other hand, small, round and granular-like particles are produced. These particles are also deposited in the cavity and on the unmachined surface, but they cannot be removed by suction.

Ablation with single-beams also showed that the flake-like particles were mainly generated at very short pulse durations of 400 fs, a small spot diameter of 4 µm and a high pulse overlap of 99%. For 10 ps as well as a pulse overlap of 70%-90% or a large spot diameter of 25 µm this type of particle is not observed. However, due to the low thermal damage of the surrounding material and the homogeneous ablation, exactly these parameters are interesting, producing a very large number of both particles.

A symmetrical re-deposition is observed for both particle types. In particular, the large flake-like particles deposited over the surface can cause short circuits within components, but this can be prevented by extraction. How the small particles in the nm range can be removed cannot yet be clarified at this point and requires further investigation.

With the use of multi-beams it could be shown by both arrangements of the spots that it is possible to influence the particles to a directed re-deposition. The particles can be pushed to the center of the crater by a V-shape or to one side by the shape of a flank. In the case of the flank in particular, it is possible for one side of the cavity to be almost free of particles. It is also noticeable that during multi-spot machining larger particles remain on the surface despite suction, what causes these and whether they belong to the flake-like or granular particles must be investigated further.

Also, the origin of the different particle types is still unclear and it can only be conjectured that it can also be attributed to a change in the dominant ablation mechanism. To further understand this process, time-resolved measurements by pump-probe microscopy would be useful in the next step.

By using small spot diameters, precise areas can be decoated by the sharp edge of the laser pulse, which is particularly helpful in the field of microelectronics and solar technology. When these small spot diameters are converted to a multi-spot array with the SLM, this edge steepness remains and by using several spots next to each other, the area to be ablated can be widened in a targeted manner. This makes it possible to design the precise decoating process more efficiently and also to specifically control the particle repositioning by the selected arrangement of the spots and to generate particle-free surfaces to avoid impairment like short circuits in electronics.

Acknowledgments

This research was supported by the German Federal Ministry of Education and Research (BMBF) (Forschungscampus Digital Photonic Production 13N15423). We would like to thank the Gemeinschaftslabor für Elektronenmiksoskopie, GFE of RWTH Aachen for the support and especially Professor Mayer, Fabian Mariano and Sebastian Zischke for the SEM images and the interesting and informative discussions.

References

[1] M. W. Rowell and M. D. McGehee: Energy Environ. Sci., 4, (2011) 131.
[2] A. L. Dawar and J. C. Joshi: J Mater Sci, 19, (1984) 1.
[3] M. Bender, W. Seelig, C. Daube, H. Frankenberger, B. Ocker, and J. Stollenwerk: Thin Solid Films, 326, (1998) 72.
[4] B. G. Lewis and D. C. Paine: MRS Bull., 25, (2000) 22.
[5] X. L. Trinh, T. H. Duong, and H. C. Kim: Int J Adv Manuf Technol, 89, (2017) 3681.
[6] F. Steuber, J. Staudigel, M. Stössel, J. Simmerer, and A. Winnacker: Appl. Phys. Lett., 74, (1999) 3558.
[7] M. Hoheisel, A. Mitwalsky, and C. Mrotzek: Phys. Stat. Sol. (a), 123, (1991) 461.
[8] C. Ji, D. Liu, C. Zhang, and L. Jay Guo: Nature communications, 11, (2020) 3367.
[9] Q. Bian, X. Yu, B. Zhao, Z. Chang, and S. Lei: Optics & Laser Technology, 45, (2013) 395.
[10] N. Farid, H. Chan, D. Milne, A. Brunton, and G. M. O'Connor: Applied Surface Science, 427, (2018) 499.
[11] H. W. Choi, D. F. Farson, J. Bovatsek, A. Arai, and D. Ashkenasi: Applied optics, 46, (2007) 5792.
[12] M.-F. Chen, Y.-P. Chen, W.-T. Hsiao, and Z.-P. Gu: Thin Solid Films, 515, (2007) 8515.
[13] R. Sahin and I. Kabacelik: Appl. Phys. A, 122, (2016).
[14] P. M. Harrison, N. Hay, and D. P. Hand: Applied Surface Science, 256, (2010) 7276.
[15] H.-Y. Kim, J.-W. Jeon, W. Choi, Y.-G. Shin, S.-Y. Ji, and S.-H. Cho: Materials (Basel, Switzerland), 11, (2018).

[16] M. Park, B. H. Chon, H. S. Kim, S. C. Jeoung, D. Kim, J.-I. Lee, H. Y. Chu, and H. R. Kim: Optics and Lasers in Engineering, 44, (2006) 138.
[17] G. E. Hallum, D. Kürschner, D. Redka, D. Niethammer, W. Schulz, and H. P. Huber: Optics express, 29, (2021) 30062.
[18] C. McDonnell: Pulsed laser material interaction with thin indium tin oxide films, Dissertation, College of Science, National University of Ireland Galway, 2015.
[19] S. Rapp, M. Domke, M. Schmidt, and H. P. Huber: Physics Procedia, 41, (2013) 734.
[20] R. W. Gerchberg and W. O. Saxton: Optik, 35, (1972) 237.
[21] D. Nieto, J. Arines, G. M. O'Connor, and M. T. Flores-Arias: Applied optics, 54, (2015) 8596.

(Received: June 24, 2022, Accepted: December 3, 2022)